Effect of charge ordering on crossplane thermal conductivity in correlated perovskite oxide superlattices

P. Thiessen,[1,*] V. Roddatis,[1] F. Rieger,[1] A. Belenchuk,[2] M. Keunecke,[3] V. Moshnyaga,[3] and Ch. Jooss[1]
[1]*Institute of Materials Physics, University of Göttingen, D-37077 Göttingen, Germany*
[2]*IIEN, Academy of Sciences of Moldova, MD2028 Chisinau, Moldova*
[3]*First Physical Institute, University of Göttingen, D-37077 Göttingen, Germany*

(Received 28 May 2018; revised manuscript received 5 October 2018; published 13 November 2018)

Lattice thermal conductivity is a sensitive probe of distortions of the translational invariance of crystalline materials. Crossplane thermal conductivity, $\kappa(T)$, was studied by the 3ω technique in superlattices, comprising orthorhombic charge/orbital ordered manganite $Pr_{0.7}Ca_{0.3}MnO_3$ and cubic $SrTiO_3$. The manganite/titanite superlattices show a peak in $\kappa(T)$ just above the charge order transition temperature $T_{CO} \sim 240\,K$ with a pronounced thermal hysteresis. This ordering peak in $\kappa(T)$ is successively suppressed with decreasing layer thickness. Our results demonstrate a minor effect of the interface density on κ, primarily visible below T_{CO}. In contrast, much higher changes in $\kappa(T)$ evolve close to T_{CO}, due to interface-induced effects on charge and orbital ordering. Our results suggest that the ordering peak in $\kappa(T)$ is a result of lattice softening above the phase transition which is modified by thickness-dependent misfit strain.

DOI: 10.1103/PhysRevB.98.195114

I. INTRODUCTION

A reduction of the crossplane lattice thermal conductivity $\kappa(T)$ in superlattices (SLs), compared to that of the individual constituting materials, was well established experimentally [1,2]. Depending on the phonon dispersion of the involved materials, layer thickness, and interface roughness, two main effects are distinguished: (i) an attenuation of phonon heat propagation due to the phononic mismatch between two different lattices, and (ii) a scattering of phonons caused by atomic distortions of the interface [3,4]. The first effect (i) is due to a coherent reflection of phonon waves at the interface, where the destructive interference of incident and reflecting phonon waves creates phonon band gaps [5]. The incoherent scattering at interfaces (ii) results in a sharp drop of the temperature at the interface, known as Kapitza resistance. However, Ravichandran *et al.* [6] demonstrated that the occurrence of coherent phonon propagation in perovskite SLs of $SrTiO_3/CaTiO_3$ (STO/CTO) and $SrTiO_3/BaTiO_3$ (STO/BTO) depends also on the scattering processes within the individual layers, yielding a crossover from incoherent to coherent phonon transport as the interface density increases. In the coherent regime, an increase of interface density can even result in an increase of $\kappa(T)$ [7].

In superlattices, where materials with strong electronic and/or electron-lattice correlations are involved, the lattice thermal conductivity is strongly affected by the change of electron-phonon and spin-phonon scattering at phase transitions. This is, e.g., reported for bulk manganite systems $Re_{1-x}(\mathrm{Sr,Ca})_xMnO_3$ (Re = La, Pr, Sm), where a significant effect of magnetic or charge/orbital order (CO/OO) phase transitions on the lattice thermal conductivity $\kappa(T)$ is observed [8–10]. At the transition into a ferromagnetic metallic state, typically a steplike increase of total thermal conductivity at $T \sim T_C$ is observed due to the electronic contribution. In contrast, the transition into antiferromagnetic order remains featureless. Remarkably, the transition into a CO/OO state is manifested by a decrease in $\kappa(T)$ which is steplike in $La_{1-x}Ca_xMnO_3$ (LCMO) ($x = 0.65$) [8] and smooth in $Pr_{1-x}Ca_xMnO_3$ (PCMO) ($x = 0.5$ and 0.3) [9,10]. Such electronic phase transitions usually are accompanied by changes in the lattice structure due to ordering of octahedral tilt and Jahn-Teller (JT) distortions, both affecting the local Mn-O bond distances. Remarkably, a unique decrease of κ with the octahedral distortion, $D = \frac{1}{3}\sum_1^3 |\frac{u_i-\bar{u}}{\bar{u}}| \times 100$ was found [8]. Here, u_i are the different Mn-O bond lengths within a MnO_6 octahedra and $\bar{u}$ is their average. Depending on whether the CO transition is rather sharp or smeared out by nanoscale phase separation, the changes in $\kappa(T)$ are only observed just below T_{CO} [8,11] or in a larger temperature range around T_{CO} [9], respectively.

In thin films and superlattices of correlated manganites, the interfaces can have a strong impact on the electronic and structural properties. For example, the epitaxial misfit actuated by interfaces can strongly affect the phase transitions. In $Pr_{0.5}Ca_{0.5}MnO_3$ thin films grown on $SrTiO_3$ (100), the colossal magnetoresistance (CMR) evolving in the CO/OO phase is shifted to lower temperatures with decreasing the film thickness t and is entirely suppressed at $t \leqslant 15$ nm [12]. It seems likely that the misfit strain as well as preparation-induced octahedral disorder can strongly influence the CO/OO phase, as the annealing of $Pr_{0.68}Ca_{0.32}MnO_3$ thin films, grown by sputtering or pulsed laser deposition, resulted in a recovery of CO phase transition [13].

Here, we report the crossplane thermal conductivity in SLs of orthorhombic $Pr_{0.67}Ca_{0.33}MnO_3$ (PCMO) and cubic STO,

---

[*] Present address: Institute of Physics, University of Hamburg, D-22761 Hamburg, Germany.

TABLE I. Bilayers and heterostructures for measurements of crossplane thermal conductivity, (T), were prepared by pulsed laser deposition (PLD), metalorganic aerosol deposition (MAD), and ion beam sputtering (IBS). The c-axis lattice parameters of PCMO layers in MAD SLs were obtained from simulations of x-ray diffraction (XRD) and are given in pseudocubic notation. Note that in the bulk $c_{\mathrm{PCMO}} = 0.38211$. T_p denotes the peak temperature of (T).

Sample	t PCMO/STO (nm)	SrO interfacing	c_{PCMO} (nm)	T_p (K)
PLD1	1 × (25/25)	No	0.382	270
PLD2	2 × (12.5/12.5)	No		225
PLD3	4 × (6.3/6.3)	No		200, weak
PLD4	8 × (3.1/3.1)	No	0.379	Disordered
MAD1	1 × (20/30)	No	0.377	220
MAD2	10 × (3.35/3.35)	Yes (at all interfaces)	0.382	240
MAD3	15 × (3.05/3.05)	Yes (at STO surfaces only)	0.381	240
MAD4	32 × (1.75/1.75)	Yes (at all interfaces)	0.381	Disordered
MAD5 (LSMO)	16 × (1.85/1.85)	Yes (at all interfaces)		
IBS	1 × (108/64)	No	0.387	Disordered

i.e., PCMO$_t$/STO$_t$, grown on STO(100) substrates with thicknesses of individual layers, $t = 1.75-25$ nm. Similar to the data reported for bulk manganites [8–10], we observe a drop of the thermal conductivity in the CO/OO ordered compared to the disordered state. In contrast to the bulk data, we find a peak in the thermal conductivity of our SLs at temperature T_p close or slightly above T_{CO} which shows a pronounced thermal hysteresis. Transmission electron microscopy studies of CO superlattice reflections and electric transport measurements published elsewhere [13] suggest that the peak at T_p can be assigned as the ordering peak. By decreasing the thickness of individual layers to $t < 3$ nm the ordering peak in $\kappa(T)$ vanishes. Below T_c, the $\kappa(T)$ of single-epitaxial PCMO films is smaller than that of all studied superlattices, indicating that the effect of the interfaces on $\kappa(T)$ by change of octahedral order is strongly dominating over their direct interface effect by the Kapitza resistance.

II. EXPERIMENT

A. Superlattice growth

Superlattices of PCMO/STO as well as one of $La_{0.7}Sr_{0.3}MnO_3$/STO were grown on STO(100) substrates by means of pulsed laser deposition (PLD) and metalorganic aerosol deposition (MAD). The essentially different thin film growth techniques are used because of the different kinetic energies of the impinging adatoms during the PLD and MAD growth. This allows for changing the preparation-induced octahedral disorder at essentially the same interface densities, thereby offering a strategy to control the ratio between interface and intralayer scattering in particular near the CO/OO phase transition. MAD operates close to the equilibrium growth conditions at a high oxygen partial pressure, $p_{O2} \sim 0.2$ bar. In contrast, PLD is a nonequilibrium technique with high kinetic energies of ions in the laser-pulse-induced plasma plume which can be controlled by background pressure and laser energy. Furthermore, the monolayer growth control within MAD [14,15] enables the reduction of misfit strain by SrO-interface engineering, resulting in nearly perfect SLs with flat and smooth layers. As a reference, we also included a $Pr_{0.5}Ca_{0.5}MnO_3$/STO bilayer prepared by ion beam sputtering (IBS). Since the lattice structure as well as electronic phases of PCMO with Ca doping $x = 1/3$ and $x = 1/2$ are very similar, yielding $T_{\mathrm{CO}} \approx 240$ K in both systems, the differences in the thermal conductivity can be mainly related to the density of defects in the samples. An overview on all samples is presented in Table I. The PLD-grown SLs where obtained at a laser energy density of 1.2 J/cm^2 at the target surface, oxygen partial pressure, $p_{O2} \sim 0.4$ mbar, and at a substrate temperature, $T_{\mathrm{sub}} = 750\,^{\circ}$C. The MAD-grown SLs were prepared at ambient air conditions ($p_{O2} \sim 0.2$ bar) and $T_{\mathrm{sub}} = 900\,^{\circ}$C. All data of the IBS sample are shown in the Supplemental Material [16].

Superlattices were structurally characterized by x-ray diffraction (XRD) and x-ray reflectivity, using a Bruker D8 diffractometer. The surface morphology was analyzed by using atomic force microscopy (AFM). Cross-section lamellas for transmission electron microscopy (TEM) studies have been prepared via focused ion beam (FIB) technology using a Nova NanoLab 600 (FEI, Netherlands), operated at 30 and 5 kV, and partially followed by a cleaning ion milling step in a Gatan PIPS 691. High resolution transmission electron microscopy (HRTEM), scanning transmission electron microscopy (STEM), and electron energy loss spectroscopy (EELS) studies have been performed using an aberration-corrected FEI Titan 80-300 operated at 300 kV. Bright field (BF) and high-angle annular dark field (HAADF) images have been acquired by using the STEM mode.

B. 3ω method

We applied the 3ω method for the measuring of the crossplane thermal conductivity of the SLs. The method was originally developed by Cahill in 1990 [17] for bulk materials. An extension for thin film materials was published in 1994 [18]. It uses the measurable temperature fluctuations in a Pt heater on top of the sample owing to an initially applied ac power P, to derive the thermal properties of the sample. For this work a four-pad Pt heater structure with a strip width $2b = 10\,\mu$m and a length $l = 1$ mm [see Fig. 1(a)] was deposited by ion beam sputtering with the usage of a lithographic mask. The lengths w and l were controlled by

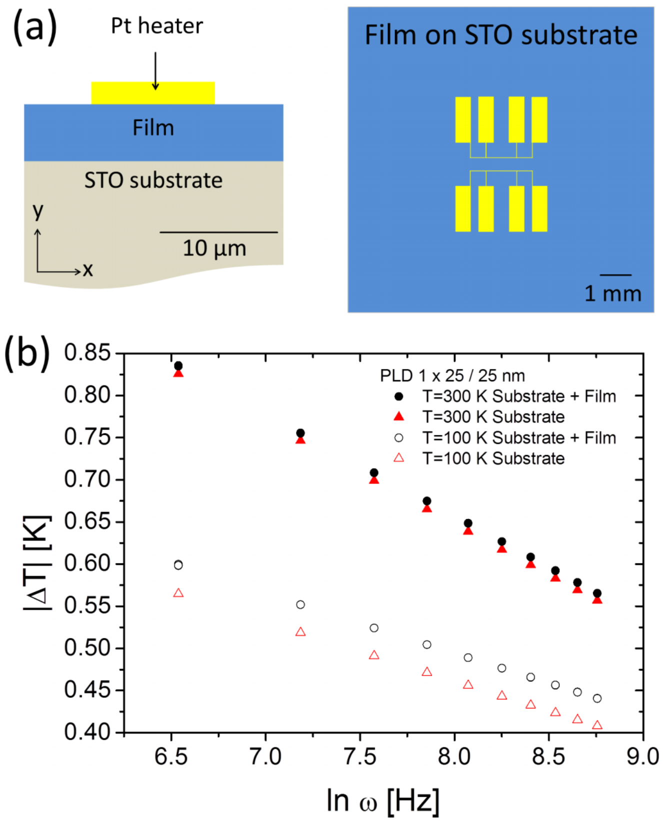

FIG. 1. (a) Schematic drawing of the measurement geometry for the 3ω method including the Pt heater structures. (b) Modulus of the temperature oscillation vs the logarithm of the frequency with a PLD PCMO/STO bilayer (measurement) and with the STO substrate only (calculated from the slope of $|T[\ln(\omega)]|$) for $T = 100$ and 300 K.

scanning electron microscopy (SEM) for each sample. The frequency dependency of the temperature fluctuations ΔT is shown in Fig. 1(b) for one PLD sample at two different temperatures.

In order to avoid the fragile measurement of phase shifts for the separation of in-phase and out-of-phase contributions to $\Delta T(\omega)$, the frequency dependence of the measured absolute value $|\Delta T|$ is analyzed for the determination of the crossplane thermal conductivity. Following the work of Borca-Tasciuc *et al.* [19], one yields

$$|\Delta T(\omega)| = \left| -\frac{I_0 V_{1\omega}}{l\pi\kappa_{S,y}} \int_0^\infty \frac{\sin^2(kb)}{(kb)^2 A\psi(\omega)} dk + \Delta T_F \right|,$$

with

$$\psi(\omega) = \sqrt{\eta_S k^2 + \frac{i2\omega(\rho c_p)_S}{\kappa_{S,y}}},$$

$$A = \frac{htc - \kappa_{S,y}\psi \tanh(\psi t_S)}{\kappa_{S,y}\psi - htc \tanh(\psi t_S)}.$$

Here, $\kappa_{S,y}$ is the substrate heat conductivity normal to the surface, $\Psi(w)$ is the Fourier transformed thermal diffusion length inside the substrate, and $\eta_S = \kappa_{S,x}/\kappa_{S,y}$ is the substrate's thermal anisotropy ($\eta_S = 1$ for STO substrates).

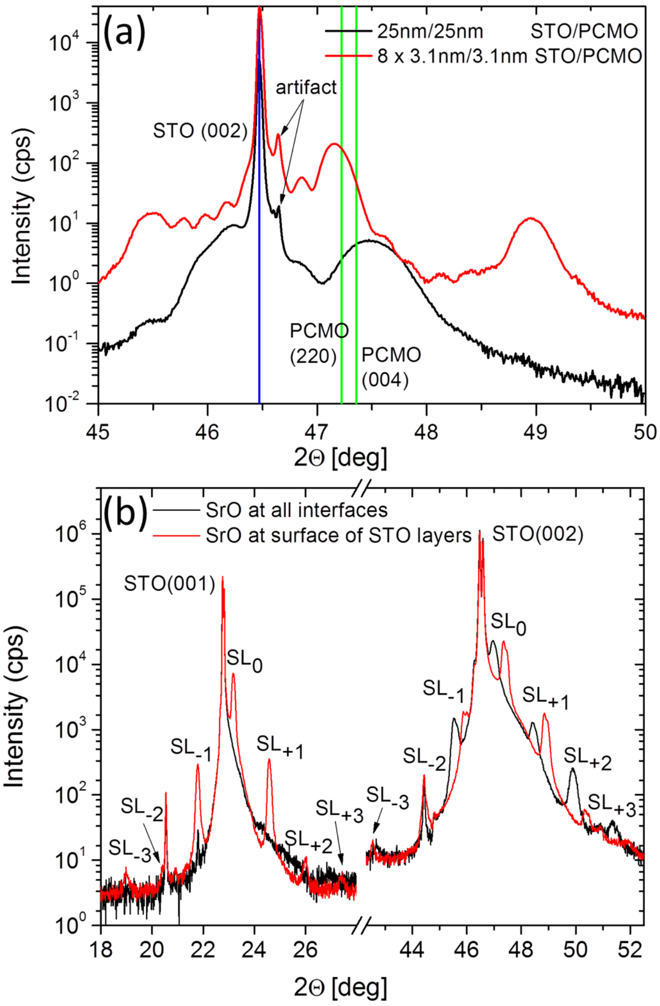

FIG. 2. XRD patterns in θ-2θ geometry of the PLD and MAD samples. For the PLD samples (a) exemplary patterns are shown for the bilayer and for the 8×3.1 nm/3.1 nm superlattice close to the (002) $SrTiO_3$ substrate reflection. The green and blue vertical lines express the expected 2θ angles for unstrained STO and PCMO single crystals, respectively. (b) Comparison of a 10×3.3 nm/3.3 nm MAD SL with additional SrO monolayers inserted at all interfaces (black) and a 14×3.2 nm/3.2 nm MAD SL, where SrO is added at the surface of STO layers only (red). PLD and IBS layers are measured by using copper $\alpha_1 = 0.154\,06$ nm radiation and MAD layers by copper α_1 and $\alpha_2 = 0.154\,18$ nm.

Furthermore, $(\rho c_p)_S$ represents the substrates thermal mass and A the backside boundary condition, depending on the thickness t_S of the substrate. For the latter the heat transfer coefficient $htc = 2.5 \times 10^4\ \mathrm{W/m^2\,K}$ is determined from test measurements.

For the final determination of the crossplane thermal conductivity of the superlattice κ we used the following formulas derived from Ref. [20] as shown in the Supplemental Material of Ref. [21]:

$$\kappa = \sqrt{\frac{1}{4}\Xi^2 + \frac{\eta_S}{\eta_F}\kappa_{S,y}^2} - \frac{1}{2}\Xi,$$

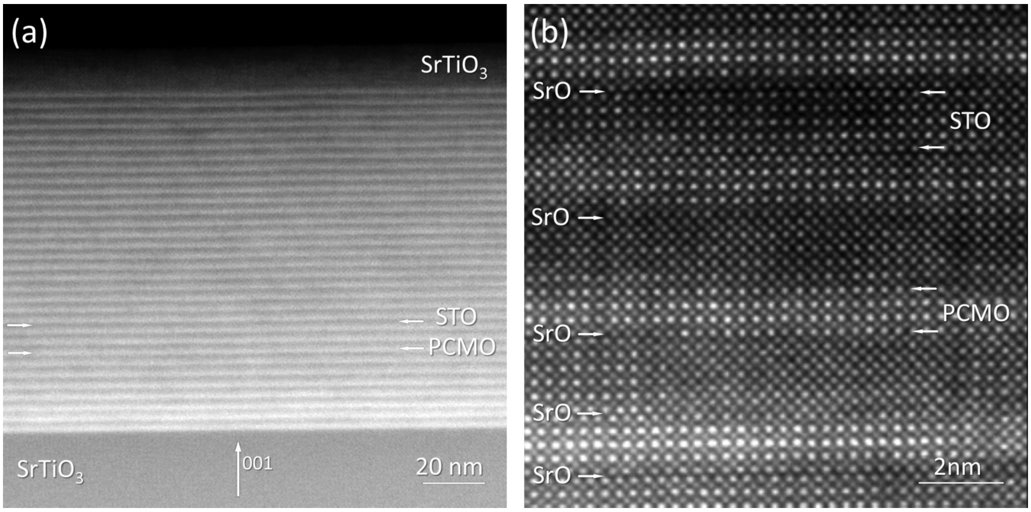

FIG. 3. STEM HAADF images of a SrO-interface-engineered PCMO/STO SL with individual PCMO and STO layer thickness $t = 1.75$ nm. (a) Overview and (b) high-resolution images with SrO monolayers at interfaces.

with

$$\Xi = \frac{\eta_S}{\eta_F}\left(\frac{2bl}{t_F P}\Delta T_F - R_{\text{ges}}\right)\kappa_{S,y}^2,$$

where t_F is the thickness of the film. The anisotropy of the films η_F has been approximated by 1 and we assumed that the Kapitza resistances between heater and film and film and substrate are negligible; that is, $R_{\text{ges}} = 0$. The crossplane thermal conductivity $\kappa(T)$ was measured in the temperature range $T = 40-370$ K. The samples are covered by an electrically insulating STO film with thickness $t = 20$ nm in order to avoid an electrical shortcut between the Pt heater and the SL.

III. EXPERIMENTAL RESULTS

The out-of-plane lattice parameters of the SL on STO (100) as well as the coherence of the lattice were studied by x-ray diffraction. Exemplary results are shown in Fig. 2. For the 25/25 nm PLD bilayer, the STO (002) peak indicates out-of-plane compressive strain of ~1% and is well separated from the PCMO (004)/(220) reflections. For the 3.1/3.1 nm SL the STO and PCMO peaks cannot be separated, indicating a heavily strained state. HAADF STEM images of both films are shown in Fig. 1S in the Supplemental Material [16].

MAD-grown interface-engineered SLs with very low interface roughness show satellite peaks up to the third order of diffraction close to the STO(001) and STO(002) peaks. Remarkably, a suppression of odd SL peaks close to the STO(100) and STO(300) peaks was observed for $t < 3$ nm, if a SrO monolayer was grown on each interface.

For all MAD samples, the SL period given in Table S1 [16] was determined by fitting of the SL peaks both in XRD and x-ray reflectivity (not shown). For the PLD SLs, the thicknesses of the individual layers were determined by cross-section STEM. The XRD of different SLs reveals the out-of-plane pseudocubic PCMO lattice constants, varying in the range of $c = 0.375-0.382$ nm (see Table I); the pseudocubic lattice parameter of PCMO ($x = 0.33$) single crystals is $c = 0.382$ nm. Since the change of lattice parameter due to preparation-induced octahedral disorder and epitaxial misfit strain cannot be separated, we did not apply a biaxial strain model to determine the in-plane strain.

Interfacing the PCMO/STO SL via an additional SrO monolayer results in nearly perfect SLs with flat and smooth layers as visible in Fig. 3, where the structure of the interface-engineered SL with additional SrO layer grown on each PCMO/STO interface is presented by low-magnification and high-resolution high-angle annular dark field (HR HAADF) STEM imaging. The images of a PCMO/STO superlattice demonstrate a nearly perfect SL architecture with 32 flat and smooth PCMO/STO double layers. Without SrO interfacing, the accumulation of stress in thin PCMO layers leads to the bending of layers upon increasing their number, finally yielding macroscopic growth defects and a large surface/interface roughness (see Fig. S2 in the Supplemental Material [16]). The SrO monolayers artificially create stacking faults in the system, presumably contributing to the relaxation of misfit strain (see also Fig. S3 in the Supplemental Material [16]).

In order to analyze the effect of the STO insulation layer (IL) on the data, we subtracted the contribution of the electrically isolating top STO layer with thickness of $t = 20$ nm, from the measured $\kappa(T)$ of PLD- and MAD-grown SLs in Figs. 4(b) and 4(d), using the series resistance model:

$$\frac{1}{\kappa(T)} = \frac{t}{t_{\text{SL}}}\frac{1}{\kappa_{\text{SL}}(T)} + \frac{t}{t_{\text{IL}}}\frac{1}{\kappa_{\text{IL}}(T)}.$$

The application of the series resistance model is justified if the phonon mean free path of the SL and in the IL is smaller than the respective thicknesses; i.e., $\lambda_{\text{MFP,SL}} < t_{\text{SL}}$ and $\lambda_{\text{MFP,IL}} < t_{\text{IL}}$. Both conditions apply as analyzed in the Discussion section of this paper. Since the IL contribution could not be measured for all SLs studied in this article, we used for the correction of the PLD SLs the data of a sputtered STO thin film with an out-of-plane strain of 0.62% [shown in Fig. 4(b)]. Magnitude and temperature dependence of $\kappa(T)$ are very similar to that of PLD STO films of similar

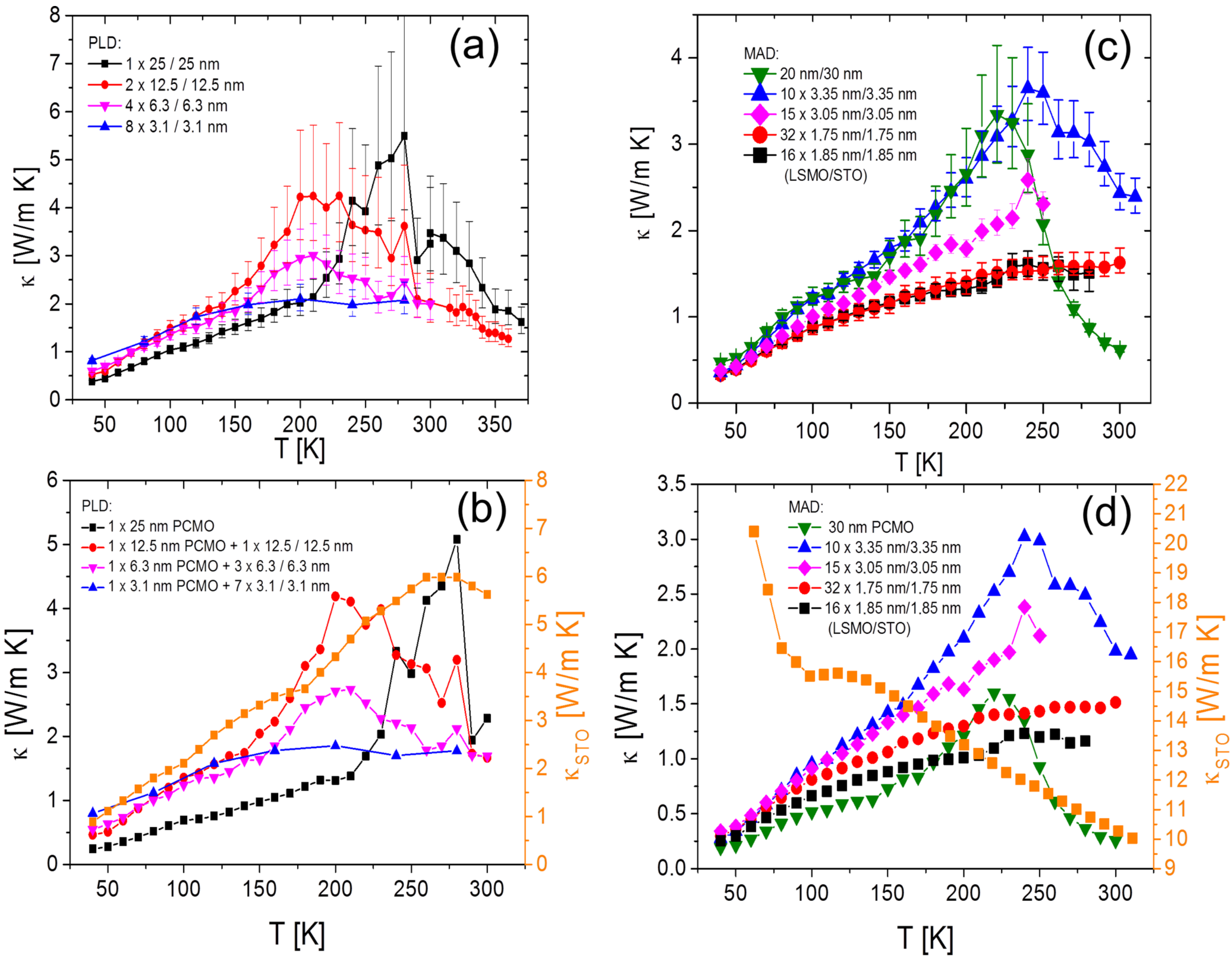

FIG. 4. Temperature dependences of thermal conductivity, $\kappa(T)$, of PLD- (a) and MAD- (c) grown SLs with different thicknesses of individual layers, $t = 1.75$–25 nm, and almost constant total film thickness, $t_\Sigma = 50$ nm, for PLD samples and different $t_\Sigma = 50$–112 nm, for MAD SLs. One can see a peak feature in $\kappa(T)$ for PLD-grown SLs with $t \geqslant 6$ nm and for MAD-SLs with $t \geqslant 3$ nm. Moreover, the peak temperature, T_p, shifts to lower temperatures with decreasing t. In contrast, for SLs with very thin layers, i.e., $8 \times (3.1/3.1$ nm) for PLD and $32 \times (1.75/1.75)$ and $16 \times (1.85/1.85)$ for MAD, no peak in $\kappa(T)$ was observed. They show for $T > 150$ K an almost temperature-independent and small, $\kappa < 1$, thermal conductivity.

strain in Oh *et al.* [22] which were grown at a laser energy density of 1.2. J/cm^2. For the correction of the MAD SLs, we used single-crystalline STO data from our substrates shown in Fig. 4(d). This can be justified by the result of Oh *et al.*, that $\kappa(T)$ of MBE-grown STO thin films is very similar to single-crystal data. Both MBE and MAD are growth techniques close to thermal equilibrium. The subtraction of the IL contribution changes the magnitude of the $\kappa(T)$ of the SLs, but it does not strongly change the $\kappa(T)$ progression and does not at all change the trends of suppressing the ordering peak with decreasing layer thickness.

Remarkably, the bilayer with the thickest PCMO layer, $t = 25$ nm, shows the lowest thermal conductivity at low temperatures, $\kappa(T < T_p)$. This can be attributed to the fact that the thermal conductivity of PCMO ($\kappa = 0.5$–$1.5\,\mathrm{W\,m^{-1}\,K^{-1}}$) for $T < T_p$ is much smaller than that of STO, $\kappa = 10$–$20\,\mathrm{W\,m^{-1}\,K^{-1}}$. Our obtained $\kappa(T < T_p)$ values for the PCMO thin film, corrected by the IL layer, are only slightly lower than that of a polycrystalline sintered PCMO material at the same doping level (Ref. [10]). This indicates that the thermal conductivity is limited by the phonon transport within the layer and not mainly by the interface scattering. The $\kappa(T)$ of the MAD bilayer and interface-engineered SLs [see Figs. 4(b) and 4(d)] also show a decrease of the peak amplitude with decreasing layer thickness. However, in contrast to the PLD-grown heterostructures, the T_p for the 3.35- and 3.05-nm-thick layers are even slightly enhanced compared to that of the bilayer. The SL with thinnest layers, i.e., $32 \times 1.75/1.75$ nm, displays no peak in $\kappa(T)$ and exhibits the lowest absolute values of $\kappa(T) < 1$ for $T < T_p$ as compared to other SLs. Remarkably, the $\kappa(T)$ of a MAD-grown $\mathrm{La_{0.7}Sr_{0.3}MnO_3}$/STO $16 \times (1.85\,\mathrm{nm}/1.85\,\mathrm{nm})$ SL, included for reference, is very similar to that of the thinnest PCMO/STO SL. This suggests that interface scattering becomes important for the phonon thermal transport for SLs with thicknesses of individual layer $t \leqslant 2$ nm.

In addition to the interface scattering and interface-induced effects on the octahedral order, the effect of preparation-induced disorder on the CO/OO transition must be taken into account. We have demonstrated this effect in Fig. S4 in the Supplemental Material [16], where the effect of increasing laser energy on $\kappa(T)$ is demonstrated for PLD-grown films. With increasing the laser energy the peak in $\kappa(T)$ vanishes and thermal conductivity decreases. Furthermore we compare the $\kappa(T)$ of PLD and MAD bilayers with a heavily strained ion-beam-sputtered PCMO/STO bilayer (Figs. S5 and S6 in the Supplemental Material [16]). Despite the large thickness, the STO and PCMO peaks are very close, thus indicating a strong change in lattice parameter due to a high degree of preparation-induced disorder, caused by the impact of high-energy ions (Ref. [23]). This results in a featureless $\kappa(T)$.

The CO/OO phase transition in PCMO is of first order [24], meaning that a metastable state with coexistence of ordered and disordered nanoscale domains [25] and a pronounced thermal hysteresis [26] is present in the vicinity of the phase transition. Nucleation of ordered (disordered) domains from the disordered (ordered) phase requires undercooling (superheating). The volume fraction of the ordered phase thus strongly depends on the thermal history of the sample [27]. Indeed, Fig. 5 shows a pronounced thermal hysteresis in $\kappa(T)$ for the MAD bilayer. The ordering peak in $\kappa(T)$ at T_p is much higher in the heating run as compared to the cooling run. We do not see a significant shift in the peak position in the "cooling" and "warming" curve of the bilayer, likely because of a broad $\kappa(T)$ distribution, pointing out a smeared CO transition, which has not been detected in the resistivity measurements (not shown). The jump of $\kappa(T)$ at $T \approx 180$ K by cooling resembles electric-field-induced jumps in the electric resistivity of PCMO thin films, observed at $T = 170-180$ K [28], and interpreted as a sudden reorganization of CO domains under combined action of thermal and misfit stresses in the films [28]. The thermal hysteresis of $\kappa(T)$ is less pronounced in the interface-engineered MAD SL with thinner individual layers, e.g., the $10 \times (3.35/3.35$ nm), shown in Fig. 5(b). This may indicate an incipient suppression of the CO/OO.

In Fig. 6 we present results of selected area electron diffraction (SAED) on a MAD-grown PCMO/STO bilayer. One can see the appearance of the CO superstructure peaks $[0, 1/2(n+1), 0]$, for $n = 0, 1, 2, \cdots$ at temperatures $T \leqslant T_{\mathrm{CO}} \sim 220$ K, in close agreement with the peak in $\kappa(T)$ in Fig. 4. A plane-view electron-transparent TEM specimen was prepared in order to increase the usable PCMO area for SAED. Due to the presence of alternating twin domains with the c axis perpendicular to the substrate, apparently the superstructure peaks are visible in both a^*- and b^*-crystallographic directions. The thermal hysteresis of the fraction of the CO phase can be clearly seen in the SAED experiments, where the superstructure peaks become visible below $T = 180$ K for cooling, whereas for warming up from 80 K, they remain visible up to a temperature above 220 K.

IV. DISCUSSION

Our experimental results establish a correlation between a peak in $\kappa(T)$ at T_p and the thickness of individual PCMO layers. Temperature-dependent electron diffraction at the MAD bilayer reveals a charge order phase transition at $T_{\mathrm{CO}} \approx 220-240$ K which well agrees with the peak in $\kappa(T)$ at $T_p \approx 220$ K. Electric transport measurements of our PLD and IBS PCMO films reveal onset of CO below $T_{\mathrm{CO}} \approx 240$ K, where the ordering degree depends on preparation-induced disorder [13]. Although we cannot directly prove the presence or absence of CO for thin PCMO in the SL by SAED due to the lack of diffracted volume, the shift of T_p with decreasing t for the PLD SLs supports the interpretation that T_p is connected to CO. Also for MAD, all SLs with thickness $t \geqslant 3$ nm, or in other words, $t \geqslant 7$ unit cells (u.c.), show a peak in $\kappa(T)$ at $T_p \sim T_{\mathrm{CO}}$, i.e., they behave similarly to the PCMO thin films with $t_{\mathrm{PCMO}} = 20-30$ nm. We will argue below that T_p may be related, rather, to the onset of the CO transition than to a fully developed CO state due to lattice softening at the phase transition.

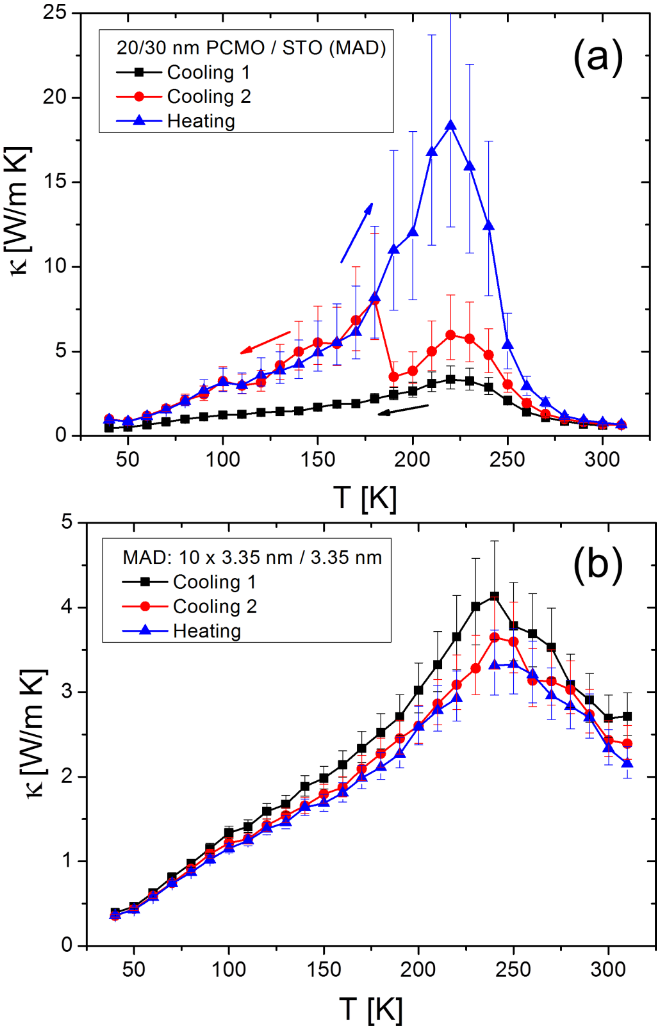

FIG. 5. Thermal hysteresis of $\kappa(T)$ of the MAD-grown PCMO/STO bilayer (a) and a $10 \times (3.35$ nm$/3.35$ nm) SL (b).

An important aspect for the understanding of the thermal conductivity is the strain state of the films. As one can see from Table I, the peak in $\kappa(T)$ does not simply correlate with the out-of-plane lattice constant of PCMO layers as they show very different lattice parameters, $c = 0.375-0.382$ nm. Since the lattice parameter is not only affected by the misfit strain

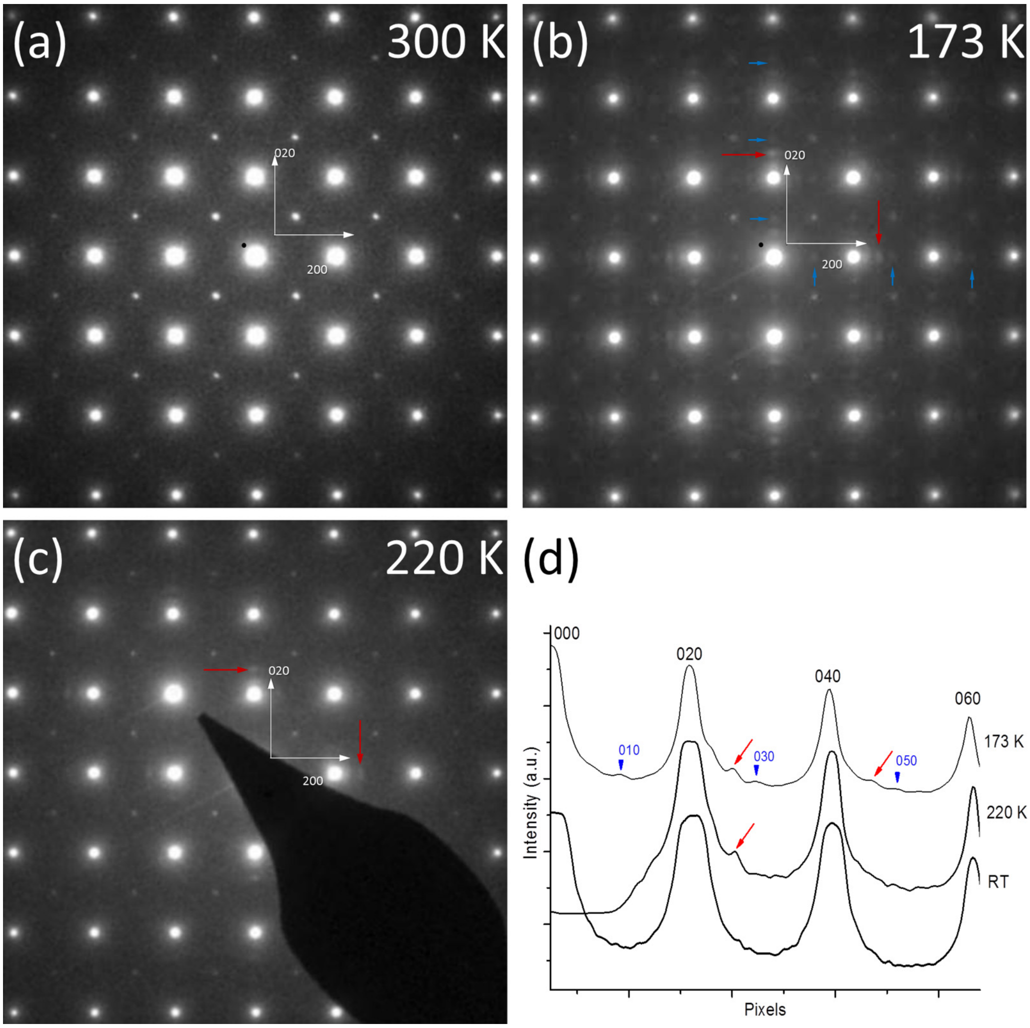

FIG. 6. Selected area electron diffraction plane-view images of the MAD-grown PCMO/STO bilayer for a charge disordered state at $T = 300\,\mathrm{K}$ (a), a charged ordered state at $T = 170\,\mathrm{K}$ after cooling down from $T = 300\,\mathrm{K}$ (b), and charged ordered state at $T = 220\,\mathrm{K}$, obtained after warming up from $T = 80\,\mathrm{K}$ (c).

but also by octahedral disorder and point defects, a simple correlation between T_p and the c lattice parameter cannot be expected. The observed decrease of T_p with decreasing layer thickness in the PLD SL at $t \approx 12\,\mathrm{nm}$ well agrees with the critical thickness, $t = 15\,\mathrm{nm}$, observed in Ref. [12]. Since the elastic modulus of STO is much bigger than that of PCMO ($E_{\mathrm{STO}} = 267$ GPa [29] and $E_{\mathrm{PCMO}} = 70$ GPa [30] at 300 K), the STO lattice can be assumed as quasirigid, whereas the PCMO lattice has to be adjusted to the STO. Without interface engineering, the in-plane lattice parameter of PCMO has to adapt to $a_{\mathrm{STO}} = 0.39\,\mathrm{nm}$, visible in a decrease of the out-of plane lattice parameter. JT stress relaxation by changing the lattice parameters, which is active for bulk PCMO, is reduced in a thin epitaxial PCMO layer sandwiched in between two rigid STO layers. In contrast, the ordering peak in interface-engineered MAD-PCMO SL is visible down to thicknesses of $t \approx 3\,\mathrm{nm}$. This indicates that SrO-interface engineering of SLs allows the disruption of the octahedral connections between PCMO and STO and thus a partial relaxation of strain in about 3.5 nm = 9 u.c.-thick PCMO layers, where the ordering peak is still visible. Only in the 1.75-nm thin interface-engineered MAD layer, a complete suppression of the ordering peak is visible. This indicates a full suppression of the first-order CO phase transition. Note that at such small thicknesses the odd SL satellite peaks in XRD become even forbidden due to the almost cubic structure of PCMO and the $a_{pc}/2$ displacement at the interface induced by the SrO layer.

In the MAD and PLD bilayers, the measured $\kappa(T)$ close to T_P is surprisingly high, in particular, in the warming run of the thermal cycle, $\kappa(T_p) \approx 18$ W/m K [see Fig. 5(a)]. The reliability of the hysteresis data is proven by the simultaneous determination of the $\kappa(T)$ of the STO substrate using the slope of $\Delta T[\ln(\omega)]$ and is presented in the Supplemental Material [16] in Fig. S7c. The high $\kappa(T)$ exceeds typical values of thermal conductivities for bulk manganites, $\kappa(T_p) \approx 2.5\text{--}10$ W/m K [24–26]. Due to rather high octahedral distortions, $D \approx 0.4\%$ [8], PCMO is expected to have a thermal conductivity at the lower end. Considering only the static distortions, one would expect a decrease of the $\kappa(T)$ in the CO/OO disordered state above T_{CO}, compared to the ordered state. Consequently, an effect which could increase $\kappa(T)$ must be taken into account for the interpretation of the hysteresis.

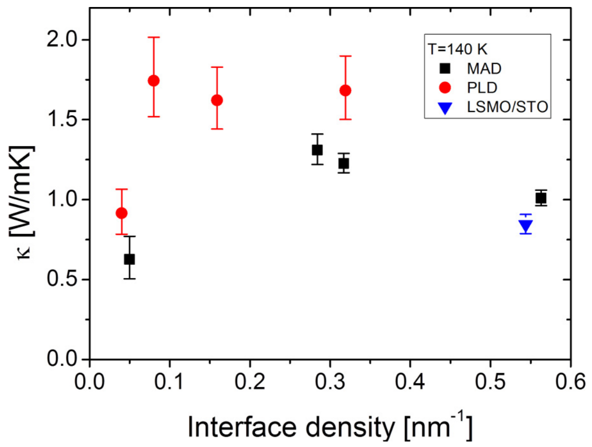

FIG. 7. Thermal conductivity of the PCMO/STO and LSMO/STO superlattices as a function of the interface density at $T = 140$ K. All data are corrected by the contribution of the STO insulation layer as described in the text.

We suggest that the combined effect of internal stress and lattice softening at temperature $T \gtrsim T_{\mathrm{CO}}$ may explain the significant increase of $\kappa(T)$ at temperatures close to T_{CO}. The shear modulus of PCMO drops smoothly from $G = 43.9$ GPa at room temperature down to 40 GPa at $T = 240$ K and then starts to steeply increase at lower temperatures in the CO phase [31] (see also Ref. [32] for $(\mathrm{La}_{0.6}\mathrm{Pr}_{0.4})_{0.7}\mathrm{Ca}_{0.3}\mathrm{MnO}_3$). Lattice softening which sets in for $T > T_{\mathrm{CO}}$ is increasing the density of long-wavelength acoustic phonon modes and thus can increase the thermal conductivity. This may be connected to a temperature-dependent maximum in the relaxation time as observed in the ultrasonic measurements in Ref. [31]. We suggest that the peak in $\kappa(T)$ observed in thin films with $t = 3$–30 nm is thus a combined result of lattice softening and enhancement of the phonon mean free path, influenced by misfit strain. It is absent in thin films with $t < 3$ nm and in films with preparation-induced strong disorder because the CO/OO phase transition is suppressed.

The suppression of the ordering peak in $\kappa(T)$ with decreasing manganite thickness is reflected in an unusual dependence of κ on the interface density, $\eta = 1/t$. Figure 7 displays $\kappa(\eta)$ for $T = 140$ K (for $T = 200$ K see Fig. S8 in the Supplemental Material [16]). At this temperature, the influence of the hysteresis on $\kappa(T)$ is minor, thus allowing the quantification of the effects originating from the Kapitza resistance of the interfaces. Remarkably, $\kappa(T = 140\,\mathrm{K})$ in bilayers and SLs is higher compared to PCMO thin films and bulk PCMO. This is, first of all, the result of the higher STO thermal conductivity. Furthermore, a partial suppression of octahedral tilt and JT distortions in PCMO thin films which are adapting the cubic STO structure due to misfit strain can also increase the mean free path l_{mfp} compared to bulk PCMO. Furthermore, for $\eta > 0.35\,\mathrm{nm}^{-1}$, κ decreases with increasing interface density for the MAD-grown interface-engineered SLs. We attribute this decrease to the contribution of interface phonon scattering. Indeed, SrO monolayers introduced at the interfaces (Fig. S3 in the Supplemental Material [16]) act as strong phonon scatters as was revealed on SrO-rich STO layers [33].

The absence of a drop of $\kappa(T = 140\,\mathrm{K})$ for $\eta < 0.35\,\mathrm{nm}^{-1}$ compared to the bulk value is quite well understandable, taking into account the actual magnitude of the thermal conductivity of the individual materials. As PCMO exhibits an intrinsically low κ, the presence of an additional incoherent scattering at the interfaces does not play a role. Furthermore, coherent phonon effects at interfaces are only relevant if the mean free path of a mode is larger than the interface-interface distance [4,34]. A rough estimate of the mean free path l_{mfp} at $T = 140$ K for PCMO layers, derived from the kinetic gas theory, gives $l_{\mathrm{mfp,PCMO}} = 3k_{\mathrm{PCMO}}/(c_V \cdot v_S)$. Using the thin film κ_{PCMO} from Fig. 5, the specific heat C_V from Ref. [35], and the effective velocity of sound from Ref. [36], one estimates a phonon mean free path in PCMO as small as $l_{\mathrm{mfp,PCMO}} = 3.6$ Å. Although kinetic gas theory often underestimates the phonon mean free path, it gives the right order of magnitude in isotropic materials. It is below the individual layer thickness t achieved in this work. On the other hand, using the same approach for STO with $\kappa_{\mathrm{STO}} = 9.5$ W/m K for a PLD thin film from Ref. [22], C_V from calorimetric measurements on STO substrates, and v_S from Ref. [37], one gets a mean free path, $l_{\mathrm{mfp,STO}} = 2.9$ nm for STO. This suggests that interface scattering is significant for the thermal conductivity of STO layers in SLs with $\eta > l^{-1}_{\mathrm{mfp,STO}} = 0.34\,\mathrm{nm}^{-1}$, which agrees quite well with the observations in Fig. 7.

In summary, a maximum of the crossplane thermal conductivity in strongly correlated PCMO/STO SLs close to the charge ordering transition in PCMO is demonstrated depending on the thickness and interface engineering of the individual films in the SL. We suggest that the ordering peak of $\kappa(T)$ is enhanced in thin films by the effect of misfit stress on CO/OO related phonon softening and is absent in ultrathin films due to suppression of the CO/OO phase transition. The critical thickness strongly depends on the interface engineering. In contrast to previous SL studies, we found that the effect of interface scattering on $\kappa(T)$ is secondary compared to the tuning of charge/orbital order by interfaces in a large temperature range.

ACKNOWLEDGMENTS

The authors acknowledge financial support from Deutsche Forschungsgemeinschaft (DFG) via SFB 1073 (Projects A02, B02, and Z02), and the DFG Projects Grant No. JO 348/12-1 and DFG Priority Program SPP-1386.

---

[1] W. S. Capinski, H. J. Maris, T. Ruf, M. Cardona, K. Ploog, and D. S. Katzer, Phys. Rev. B **59**, 8105 (1999).

[2] S. T. Huxtable, A. R. Abramson, Ch.-L. Tien, A. Majumdar, Ch. LaBounty, X. Fan, G. Zeng, J. E. Bowers, A. Shakouri, and E. T. Croke, Appl. Phys. Lett. **80**, 1737 (2002).

[3] E. T. Schwarz and R. O. Pohl, Rev. Mod. Phys. **61**, 605 (1989).

[4] G. Chen, Phys. Rev. B **57**, 14958 (1998).

[5] M. V. Simkin and G. D. Mahan, Phys. Rev. Lett. **84**, 927 (2000).

[6] J. Ravichandran, A. K. Yadav, R. Cheaito, P. B. Rossen, A. Soukiassian, S. J. Suresha, J. C. Duda, B. M. Foley, C.-H. Lee,

Y. Zhu, A. W. Lichtenberger, J. E. Moore, D. A. Muller, D. G. Schlom, P. E. Hopkins, A. Majumdar, R. Ramesh, and M. A. Zurbuchen, Nat. Mater. **13**, 168 (2013).

[7] M. N. Luckyanova, J. Garg, K. Esfarjani, A. Jandl, M. T. Bulsara, A. J. Schmidt, A. J. Minnich, S. Chen, M. S. Dresselhaus, Z. Ren, E. A. Fitzgerald, and G. Chen, Science **338**, 936 (2012).

[8] J. L. Cohn, J. J. Neumeier, C. P. Popoviciu, K. J. McClellan, and T. Leventouri, Phys. Rev. B **56**, R8495 (1997).

[9] J. Hejtmanék, Z. Jirák, Z. Arnold, M. Maryško, S. Krupička, C. Martin, and F. Damay, J. Appl. Phys. **83**, 7204 (1998).

[10] M. Ikebe, H. Fujishiro, S. Kanoh, and H. Yamazaki, J. Magn. Magn. Mater. **272-276**, 1798 (2004).

[11] J. Hejtmanék, Z. Jirák, M. Maryško, C. Martin, A. Maignan, M. Hervieu, and B. Raveau, Phys. Rev. B **60**, 14057 (1999).

[12] W. Prellier, Ch. Simon, A. M. Haghiri-Gosnet, B. Mercey, and B. Raveau, Phys. Rev. B **62**, R16337(R) (2000).

[13] J. Hoffmann, P. Moschkau, J. Norpoth, and Ch. Jooss, Mater. Res. Express **1**, 046403 (2014).

[14] M. Jungbauer, S. Hühn, R. Egoavil, H. Tan, J. Verbeeck, G. Van Tendeloo, and V. Moshnyaga, Appl. Phys. Lett. **105**, 251603 (2014).

[15] A. Belenchuk, O. Shapoval, V. Roddatis, V. Bruchmann-Bamberg, K. Samwer, and V. Moshnyaga, Appl. Phys. Lett. **109**, 232405 (2016).

[16] See Supplemental Material at http://link.aps.org/supplemental/10.1103/PhysRevB.98.195114 for additional TEM, x-ray diffraction, and thermal conductivity data.

[17] D. G. Cahill, Rev. Sci. Instrum. **61**, 802 (1990).

[18] D. G. Cahill, M. Katiyar, and J. R. Abelson, Phys. Rev. B **50**, 6077 (1994).

[19] T. Borca-Tasciuc, A. R. Kumar, and G. Chen, Rev. Sci. Instrum. **72**, 2139 (2001).

[20] T. Tong and A. Majumdar, Rev. Sci. Instrum. **77**, 104902 (2006).

[21] F. Rieger, K. Kaiser, G. Bendt, V. Roddatis, P. Thiessen, S. Schulz, and C. Jooss, J. Appl. Phys. **123**, 175108 (2018).

[22] D.-W. Oh, J. Ravichandran, C.-W. Liang, W. Siemons, B. Jalan, C. M. Brooks, M. Huijben, D. G. Schlom, S. Stemmer, L. W. Martin, A. Majumdar, R. Ramesh, and D. G. Cahill, Appl. Phys. Lett. **98**, 221904 (2011).

[23] S. Wiedigen, T. Kramer, M. Feuchter, I. Knorr, N. Nee, J. Hoffmann, M. Kamlah, C. A. Volkert, and Ch. Jooss, Appl. Phys. Lett. **100**, 061904 (2012).

[24] Ch. Jooss, T. Beetz, L. Wu, M. Beleggia, R. Klie, M. Schofield, Y. Zhu, S. Schramm, and J. Hoffmann, Proc. Natl. Acad. Sci. U. S. A. **104**, 13597 (2007).

[25] L. Wu, R. F. Klie, Y. Zhu, and Ch. Jooss, Phys. Rev. B **76**, 174210 (2007).

[26] W. Westhäuser, S. Schramm, J. Hoffmann, and Ch. Jooss, Eur. J. Phys. B **53**, 323 (2006).

[27] P. Moschkau, S. Schramm, J. Hoffmann, J. Fladerer, Ch. Jooss, L. Wu, and Y. Zhu, Mater. Sci. Eng. B **144**, 78 (2007).

[28] S. Schramm, J. Hoffmann, and Ch. Jooss, J. Phys.: Condens. Matter **20**, 395231 (2008).

[29] J. Hornstra and W. J. Bartels, J. Cryst. Growth **44**, 513 (1978).

[30] E was was calculated from the PCMO shear modulus $G = 43.9$ GPa (Ref. [24]) by assuming isotropy and a Poisson ratio of $\upsilon = 0.25$.

[31] M. A. Carpenter, Ch. J. Howard, R. E. A. McKnight, A. Migliori, J. B. Betts, and V. R. Fanelli, Phys. Rev. B **82**, 134123 (2010).

[32] M. Michelmann, V. Moshnyaga, and K. Samwer, Phys. Rev. B **85**, 014424 (2012).

[33] C. M. Brooks, R. B. Wilson, A. Schäfer, J. A. Mundy, M. E. Holtz, D. A. Muller, J. Schubert, D. G. Cahill, and D. G. Schlom, Appl. Phys. Lett. **107**, 051902 (2015).

[34] G. Chen, T. Zeng, T. Borca-Tasciuc, and D. Song, Mater. Sci. Eng., A **292**, 155 (2000).

[35] M. R. Lees, O. A. Petrenko, G. Balakrishnan, and D. McK. Paul, Phys. Rev. B **59**, 1298 (1999).

[36] S. Seiro, H. R. Salva, M. Saint-Paul, A. A. Ghilarducci, P. Lejay, P. Monceau, M. Nunez-Regueiro, and A. Sulpice, J. Phys.: Condens. Matter **14**, 3973 (2002).

[37] R. O. Bell and G. Rupprecht, Phys. Rev. **129**, 90 (1963).